Research Square

Preprints are preliminary reports that have not undergone peer review.
They should not be considered conclusive, used to inform clinical practice,
or referenced by the media as validated information.

Global models overestimate giant sea salt aerosol mixing ratio

Katherine L. Ackerman

klackerm@hawaii.edu

University of Hawai□i at Mānoa

Alison D. Nugent

University of Hawai□i at Mānoa

Jorgen B. Jensen

National Center for Atmospheric Research

Article

Keywords: giant sea salt aerosol, global models, aerosol production

Posted Date: April 8th, 2026

DOI: https://doi.org/10.21203/rs.3.rs-9255278/v1

License: This work is licensed under a Creative Commons Attribution 4.0 International License.
Read Full License

Additional Declarations: No competing interests reported.

Global models overestimate giant sea salt aerosol mixing ratio

Katherine L. Ackerman[1*], Alison D. Nugent[1*†] and Jørgen B. Jensen[2†]

[1*]Department of Atmospheric Sciences, University of Hawaii at Mānoa, 2525 Correa Road, Honolulu, 96822, Hawaii, USA.
[2]Earth Observing Laboratory, National Center for Atmospheric Research, 3090 Center Green Drive, Boulder, 80301, Colorado, USA.

*Corresponding author(s). E-mail(s): klackerm@hawaii.edu; anugent@hawaii.edu;
Contributing authors: jbj@ucar.edu;
†These authors contributed equally to this work.

Abstract

Giant sea salt aerosol particles (GSSA) influence Earth's radiative balance and aerosol-cloud interactions on a global scale. Both *in situ* measurements and remote sensing techniques have worked to quantify aerosol concentrations worldwide, often linking these observations to local conditions such as wind speeds and wave heights in order to develop statistical relationships or source functions. These tools are then used to estimate the broader global and vertical distributions of GSSA beyond isolated measurements.

Reanalysis products like the NASA Modern-Era Retrospective analysis for Research and Applications, Version 2 (MERRA-2), and the ECMWF Atmospheric Composition Reanalysis 4 (EAC4) are two main products that model sea salt aerosol (SSA) on a global scale. These products provide vertically resolved SSA mixing ratio estimates across five discrete bins, enabling continuous spatial and temporal coverage (3-hourly) in contrast to the point-based nature of *in situ* data.

In this study, we compare GSSA mass mixing ratio estimates from MERRA-2 and EAC4 with *in situ* measurements collected during the VOCALS (2008), ICE-T (2011), and SOCRATES (2018) aircraft-based field campaigns. Our results show that both reanalysis products significantly overestimate GSSA mass mixing ratio in both magnitude and vertical distributions throughout and above

the marine boundary layer. These discrepancies, ranging 2-4 orders of magnitude above observations on average, generate bias in studies aiming to assess the climate impact of GSSA that rely on these products to represent their global distribution.

Keywords: giant sea salt aerosol, global models, aerosol production,

1 Main

Sea salt aerosol (SSA) particles are widespread in the marine atmosphere and act as an important source of cloud condensation nuclei [1]. The largest sizes of SSA, Giant SSA (GSSA, dry radius $r_d \geq 1$ µm), are hypothesized to play critical roles in radiation budgets through direct [2, 3] and indirect effects [4, 5], as well as influence moisture and heat fluxes within the marine boundary layer (MBL) [2, 3, 6, 7]. They dominate the total mass flux of SSA and make up the largest source of uncertainty in global mass fluxes of any natural aerosol [8]. These uncertainties in their production can propagate bias in estimates of their potential aerosol forcings, impacting studies on the aerosol direct effect, aerosol-cloud-interactions, and future warming scenarios [9].

GSSA particles' role in clouds are complex. Their large sizes make them potential raindrop embryos through condensational growth alone [10, 11] and promote broadening of cloud droplet size distributions through mixing and entrainment [10, 12]. These aerosol-cloud interactions (ACI) inherently impact indirect radiative feedbacks and cloud development through the Twomey [13] (less bright clouds), Albrecht [14] (enhanced drizzle), and Semi-direct effect [15] (potentially outlasting other natural aerosol, like black carbon, during cloud burnoff). They also have implications for climate mitigation techniques such as marine cloud brightening. For example, they are hypothesized to aid in drizzle initiation within stratocumulus clouds, though with varying orders of magnitude [5, 11, 16–20], which would reduce these clouds' brightness and lifetime. These giant particles may also experience enhanced condensational growth within clouds that may result in reduced activation of smaller cloud condensation nuclei (CCN) [21, 22]. Below the clouds, they may reduce the total number of available CCN by scavenging smaller, more plentiful particles [23]. Therefore, it is important to accurately represent the global and vertical distributions of these particles in models if these products are going to be used to assess their impacts on atmospheric processes.

For decades, simply observing these particles has been challenging, with few studies capturing observations throughout the MBL [24–28]. Woodcock (1949) [29] was the first to observe a GSSA size distribution (GSSA-SD) using the impaction method and aircraft over the open ocean. Since then, many modern aircraft aerosol samplers have struggled with high loss rates due to these particles' inherently large sizes [30], or struggled with cumbersome instrumentation designs and low sampling rates [31–33]. Observations that do capture these particles typically consist of either total number concentrations [25](dominated by the particles with r_d=1 µm) or total mass [24] (dominated by particles with r_d between 2-3 µm) and use a variety of different methods

to characterize their observations; (1) chemical characterization to analyze measurements of Na^+ and Cl^- compositions of particles [34, 35], (2) fitting to a canonical size distribution, like those from Lewis and Schwartz (2004) [8] or Woodcock (1949) [25, 36–40], or (3) association with a size distribution based on physical properties such as hygroscopicity and volatility [1, 41–43], all of which have varying degrees of uncertainty and error [44]. Each approach has associated uncertainties, and ultimately, the variety in observational methods limits the comparability of studies, complicating efforts to form a unified understanding of the mechanisms that contribute to and control atmospheric concentrations of GSSA.

Using over 800 *in situ* GSSA size distributions (GSSA-SDs) collected from three field campaigns spread across the globe (VOCALS, ICE-T, and SOCRATES), we visualize the vertical mixing of GSSA particles within the MBL and lower free troposphere to understand the natural vertical distribution of these particles as a function of altitude. Then, we compare the *in situ* mass mixing ratio to the derived mass mixing ratio from MERRA-2 and EAC4 reanalysis products using the corresponding model pressure level and location. The novel sampling methodology of the GNI-system combined with the GNI-Microscope allowed for the analysis of precise and discrete observations of GSSA-SDs from $1.0 \leq r_d \leq 20.0$ µm at 0.2 µm bin width.

GSSA were observed to be well mixed throughout the MBL with sharp decreases in concentration above cloud base height for all three field campaigns. Even the largest observed particles ($r_d \geq 7$ µm), which are typically expected to settle quickly due to their size, were distributed nearly uniformly throughout the MBL on average, indicating that vertical mixing in the boundary layer can sustain GSSA aloft under a wide range of wind speeds. These results challenge assumptions of the limited mixing potential of these particles within the MBL and reinforce the importance of accounting for vertical transport when evaluating aerosol distributions in marine environments.

When the *in situ* data is compared to global reanalysis products (MERRA-2 and EAC4), both substantially overestimate GSSA mass mixing ratios ($GSSA_{\mathrm{MR}}$s), particularly at higher altitudes and stronger wind speeds. While MERRA-2 more significantly overpredicted $GSSA_{\mathrm{MR}}$s compared to EAC4, on average it appeared to more closely represent vertical mixing profiles of of these particles when compared to in situ observations for both $GSSA_{\mathrm{MR}}$ bins. However, both models consistently predicted strong vertical mixing into the free troposphere unsupported by observations. For the convective region, ICE-T, EAC4 mixes these giant particles well into the free troposphere, a phenomena not backed by observations in this study. Quantifying model performance using a logarithmic bias between the *in situ* mixing ratios and model predictions revealed that accuracy deteriorates as functions of wind speed and altitude, suggesting current source functions and vertical transport schemes are not adequately tuned for giant particles. These findings emphasize the critical need for refining aerosol parameterizations in global models to better reflect observed distributions, ultimately improving our ability to estimate their impacts on radiative forcing and cloud interactions in the MBL.

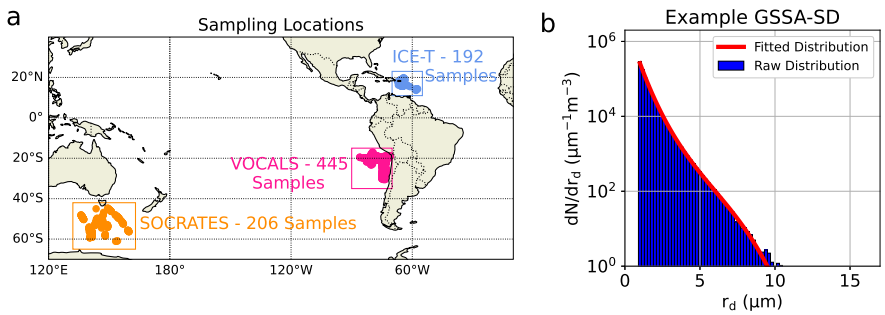


Fig. 1 (a) A map showing the three field campaigns in this study; VOCALS (pink), SOCRATES (orange), and ICE-T (light blue), along with the total number of samples utilized from each campaign, with the dots representing *in situ* sample locations. (b) shows an example GSSA-SD with the 0.2 µm r_d bin widths, and the red line is a fitted 3rd-order polynomial. These fitted red lines allow for easy comparison of histograms across different environmental conditions, such as those shown in the Extended Data.

2 Methods

2.1 Sampling of giant sea salt aerosol

2.1.1 Sample locations and field campaign background

Data in this study comes from three international field campaigns; the VAMOS-Ocean Cloud Atmosphere Land Study Regional Experiment (VOCALS, NSF/NCAR C-130 [45]), Ice in Clouds Experiment—Tropical (ICE-T, NSF/NCAR C-130), and Southern Ocean Clouds-Radiation-Aerosol Transport Experimental Study (SOCRATES, NSF/NCAR GV [46]) collected *in situ* GSSA size distributions (GSSA-SD) across a variety of altitudes using aircraft. A generalized geographic representation of each field campaign location can be found in Figure 1a with the dots representing individual sample locations, while Figure 1b shows an example GSSA-SD. These GSSA-SDs span a range of atmospheric and geographic conditions across a variety of seasons. Each campaign samples predominately within the mixed layer of the MBL, with several tens of samples taken in the free troposphere as well.

2.1.2 The Giant Nuclei Impactor methods

While these field campaigns utilize two different aircraft, the methods and processing of the GSSA-SDs remain the same, making the comparison of samples between locations possible without imposing nuanced interpretations of different aerosol collection methods. The aerosol collection in this study, created by Jensen et al. (2020) [47], relies on the impaction method of Woodcock (1949) [29] where clean slides are exposed perpendicularly to the free airstream. The GSSA particles have significant inertia compared to submicron particles, impacting themselves onto the slide as air travels around it. This method is advantageous for exclusively collecting giant particles and avoids particle breakup by impaction inside curved sample tubes [47].

Jensen et al. (2020) [47] expanded on the impaction method to build a manual NSF/NCAR Giant Nuclei Impactor (GNI) for use on NSF/NCAR aircraft. VOCALS was the first project to use the manual GNI on the NSF/NCAR C-130 aircraft with an airfoil strut to expose the slide well outside the aircraft. A double airlock was used to retain aircraft pressurization and to avoid high-speed air movement as the slide was brought back into the aircraft cabin. These methods were implemented again in 2011 for the ICE-T campaign. In 2018, this process was automated with the development of the auto-Giant Nuclei Impactor (auto-GNI, doi.org/10.26023/r267-m386v) which was used on the NSF/NCAR GV aircraft during SOCRATES. Slides for these three campaigns were exposed for approximately 10-30 s, yielding sample volumes of about 100-300 L. After collection, the slides were stored in desiccated test tubes and transported for laboratory microscope image analysis where size-distribution histograms were derived.

2.1.3 Slide analysis

Analysis of the slides collected using the above methods relies primarily on three variables; air speed (relative to the slide), dry mass of the salt particle, and ambient relative humidity (RH). Dynamic viscosity of air also plays a role, however, smaller than the aforementioned variables. The dry mass of the salt particle, RH, and relative air speed dictate the calculations of collision efficiency (CE) by controlling the total deliquesced particle mass and consequently, particle inertia. When the manual GNI and auto-GNI are deployed on a nonstationary system (i.e., a plane), the relative speed is based on the vector between the true wind and the moving system's velocity.

The weakest wind observation dictates which particle sizes can be compared across samples, and only particles with a CE>40% are used for analyses ([48, 49]). For these three studies, the GSSA-SDs are taken via aircraft where average relative wind speeds are typically $\geq$100 m s^{-1}, meaning all slides in this study impact particles as small as 1 µm r_d near 100% CE.

All resulting slides are analyzed using the microscope methods detailed in Jensen et al. (2020) [47]. This method dehydrates the initial deliquesced salt particles immediately after collection and then re-hydrates them in a closed humidified microscope chamber to $\approx$ 90% RH. When in equilibrium, the GSSA particles deposited on the polycarbonate slide grow into spherical cap drops that have a distinguishable average aspect ratio (cap height to cap base radius) of 0.85 [47]. When viewed by the microscope from above, the spherical cap drops form dark grey circles in digital grey-scale images. Circular particles with dark edges are by far the most common particle morphology. Rare circular particles with low grayscale contrast (possibly due to strong organic coating resulting in low surface tension) are not analyzed, as the cap volume cannot be reliably determined, and irregular particles (e.g., mineral dust) are also excluded based on particle morphology. Thus only round high-contrast particles assessed as sea salt droplets are included in the measured size distributions. The hemispheric droplets are converted to r_d of pure salt (density of 2200 kg m^{-3} [8]) using the conversion described in Tang et al. (1997) [50] at a bin width of 0.2 µm, providing a GSSA-SD for each sample. To be consistent with normal aerosol size distribution conventions, each GSSA-SD is normalized by the bin width, making the units concentration per bin width per volume (N μm^{-1} m^{-3}).

2.2 Giant sea salt aerosol from reanalysis products

The Modern-Era Retrospective analysis for Research and Applications, Version 2 (MERRA-2, https://doi.org/10.5067/LTVB4GPCOTK2) from the National Aeronautics and Space Administration provides reanalysis estimates of aerosol loading globally at 0.5°x 0.625° horizontal resolution and 72 vertical levels every 3-hours. Sea salt aerosol mixing ratios are provided at five separate bin widths and utilize Gong (2003) [51] as the SSSF for production [52]. In this study, we compare the last two bin widths, SS004 ($1.5 \leq r_d < 5$ µm) and SS005 ($5 \leq r_d < 10$ µm), which encompasses a complete range of observable particle sizes for the GSSA-SDs in VOCALS, SOCRATES, and ICE-T.

In addition to MERRA-2, the European Centre for Medium-Range Weather Forecasts (ECMWF) Atmospheric Composition Reanalysis 4 (EAC4) [53] is a global reanalysis product of atmospheric composition combining model data with observations. Global observations are assimilated every 12 hours, but EAC4 provides model estimates of SSA mixing ratio every 3-hours for 60 vertical levels at 0.75°x 0.75° horizontal resolution. EAC4 contains three bins of sea salt aerosol produced by Monahan (1986) [54]. EAC4 SSA mixing ratio treats these particles at an RH of 80%, or r_{80}, meaning the total mass mixing ratio ($GSSA_{MR}$) includes both the dry salt particle and deliquesced water mass at 80% RH. This means the two largest bins of original particle ranges of $0.5 < r_{80} < 5$ µm radius (AERMR02) and $5 \leq r_{80} \leq 20$ µm (AERMR03) represent bins of dry particle radius from $\approx 0.25 < r_d < 2.5$ µm (AERMR02) and $\approx 2.5 \leq r_d \leq 10$ µm (AERMR03), or a reduction in radius by a factor of 1.99 from particle radius

at 80% RH to r_{d}, unlike MERRA-2. To remove the water mass from these products in the $GSSA_{\mathrm{MR}}$, a reduction of a factor of 4.3 was applied according to Copernicus' guidance [55]. Authors recognize that the AERMR02 bin exists outside the observable range of *in situ* particles of this study ($0.25<r_{\mathrm{d}}<1$ µm), and that these sizes are inclusive of particles smaller than GSSA. However, given the majority of the mass for this bin comes from the GSSA particles rather than the submicron particles of this size range, this bin has been included in the analysis.

ECMWF Reanalysis Version 5 (ERA5, [56]) provides 1-hourly resolution and horizontal grid spacing of ≈ 25 km. Using the geographic locations, altitudes, and times from each sample, ERA5 provided additional variables such as cloud base height and 10 meter wind speed (U_{10}) for each sample to supplement variables not observed directly by the aircraft.

3 GSSA are well mixed throughout the mixed layer

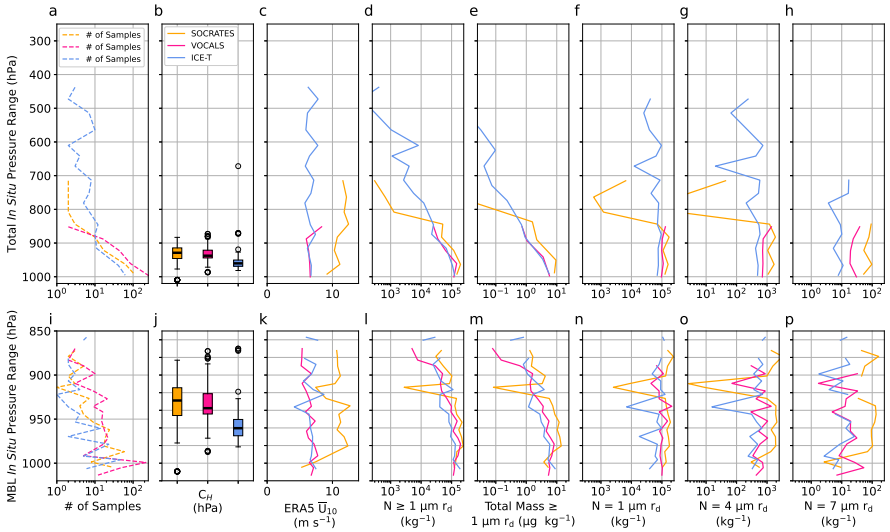


Fig. 2 Vertical profiles as a function of pressure (hPa) for the entire sampling range (first row) and approximately the MBL (second row) for each field campaign showing **(a, i)** total number of samples, **(b, j)** the 25th, median, and 75th percentiles of the Cloud Base Height (C_H) for each field campaign taken from ERA5, **(c, k)** the average U_{10} for the samples taken at each pressure level from ERA5 (m s^{-1}), **(d, l)** specific number concentration for particles $r_{\mathrm{d}} \geq 1$ µm (N kg^{-1}), **(e, m)** mass mixing ratio for particles $r_{\mathrm{d}} \geq 1$ µm (µg kg^{-1}), **(f, n)** specific number concentration for particles of r_{d} = 1-1.9 µm ($\mu\mathrm{m}^{-1}$ kg^{-1}), **(g, o)** specific number concentration for particles of r_{d} = 4-4.9 µm ($\mu\mathrm{m}^{-1}$ kg^{-1}), and **(h, p)** specific number concentration for particles of r_{d} = 7-7.9 µm ($\mu\mathrm{m}^{-1}$ kg^{-1}). The orange lines represent samples from SOCRATES, pink lines from VOCALS, and light blue lines from ICE-T. With the exception of ERA5 C_H and ERA5 $\overline{U}_{10}$ columns, all other X-axes are on a logarithmic scale.

Campaign	#	U_{10} Range (m s^{-1})	Air Temp. Range (K)	RH Range (%)	Alt. Range (m)	G-Mean$_C$ (N m^{-3})	G-Mean$_M$ (μg m^{-3})
VOCALS (2008-10-17: 2008-11-15)	445	0.5-10.2	276-291	45-93	30-2570	1.31	2.21
ICE-T (2011-07-06: 2011-07-30)	192	3.2-9.9	261-300	45-92	42-7016	1.28	2.13
SOCRATES (2018-01-15: 2018-02-24)	206	2.8-15.5	262-285	45-99	152-2734	1.32	2.48

Table 1 The campaign name and dates for the samples in this study are the first column, followed by the total number of samples (#), the estimated 10 meter wind speed range (U_{10}, m s^{-1}) taken from ERA5, the air temperature (Air. Temp. Range, K) range, relative humidity range (RH, %), as well as the *in situ* altitude range (Alt. Range, m), geometric mean for the concentration (G-Mean$_C$, N m^{-3}), and geometric mean for the mass (G-Mean$_M$, μg m^{-3}) are shown for all three field campaigns. Both geometric mean concentrations and mean masses are for GSSA particles $r_d \geq 1$ μm. All values in the table are from *in situ* observations with the exception of the estimated U_{10} wind speeds from ERA5.

Three international field campaigns (VOCALS, ICE-T, and SOCRATES) provide over 800 GSSA-SDs across a variety of altitudes and environmental conditions (Fig. 2). The GSSA-SDs demonstrate with high resolution how well particles of different sizes are mixed throughout the MBL, as well as demonstrate that concentrations drop off as these particles transition from the MBL to the free troposphere. Table 1 highlights details of all three campaigns, showing that while VOCALS contains the largest number of samples (#), SOCRATES experiences the greatest range in U_{10} and ICE-T covers the largest range of altitudes.

Figure 2 shows vertical profiles of multiple aerosol quantification metrics as a function of pressure. In the first row, these metrics extend through all sampled pressures, while the second row highlights samples close to the MBL of these geographic regions (designated approximately by cloud base height (C_H, Fig. 2j). While wind speed is expected to change as a function of pressure, the average ERA5 U_{10} ($\overline{U}_{10}$) (a variable considered important in SSA production) for samples within pressure levels for each campaign is shown to demonstrate that the $\overline{U}_{10}$ remains approximately constant among samples at different altitudes within each field campaign (Fig. 2c, k).

For all field campaigns, both $GSSA_{\mathrm{MR}}$ (µg kg^{-1} for $r_{\mathrm{d}}\geq$1 µm) and specific number concentration (N kg^{-1} for $r_{\mathrm{d}}\geq$1 µm) appear well mixed within the MBL but appear to decrease rapidly with altitude in the free troposphere. Specific number concentrations (N kg^{-1}) of three particle bins (r_{d} from 1-1.9 µm, 4-4.9 µm, and 7-7.9 µm) show similar patterns. SOCRATES observed slightly higher $GSSA_{\mathrm{MR}}$s and specific number concentrations compared to VOCALS and ICE-T, but this is potentially due to increased production in this region due to the overall elevated $\overline{U}_{10}$ during this campaign (Fig. 2c, k, Table 1). Still, there is strong agreement among these aerosol metrics for SOCRATES, VOCALS, and ICE-T despite the differences in average environment conditions between these regions.

Fewer samples contain particles with r_{d} as large as 7 µm, but these samples demonstrate that vertical mixing of these larger particles is possible to significant altitudes despite hypotheses that they have relatively short atmospheric lifetimes [8]. Extended Data Figure 1 demonstrates the strong similarity between GSSA-SDs at different altitudes within different 1 m s^{-1} U_{10} bins within each field campaign. This, in combination with the altitude averages in Figure 2, indicates that the vertical mixing of GSSA particles of sizes within this study do not appear to be an obvious function of altitude within the MBL for particles up through 7 µm r_{d}.

4 Global reanalysis products overestimate GSSA

Next, we calculate the *in situ* $GSSA_{\mathrm{MR}}$s constrained by the sizes of the two aerosol bin ranges of two global models; MERRA-2 and EAC4. The particle size ranges used to calculate the *in situ* $GSSA_{\mathrm{MR}}$ differs slightly between MERRA-2 and EAC4, but we are comparing the *in situ* $GSSA_{\mathrm{MR}}$s to the modeled $GSSA_{\mathrm{MR}}$s for particles of the same r_{d}. The two largest bins from MERRA-2 are SS004 and SS005, representing $GSSA_{\mathrm{MR}}$s for particles from $1.5<r_{\mathrm{d}}<5$ µm and $5\leq r_{\mathrm{d}}\leq 10$ µm respectively, while the two largest bins from EAC4 are AERMR02 and AERMR03 and represent particles from $0.25\leq r_{\mathrm{d}}<2.5$ µm and $2.5\leq r_{\mathrm{d}}\leq 10$ µm, respectively. Again, the observations in

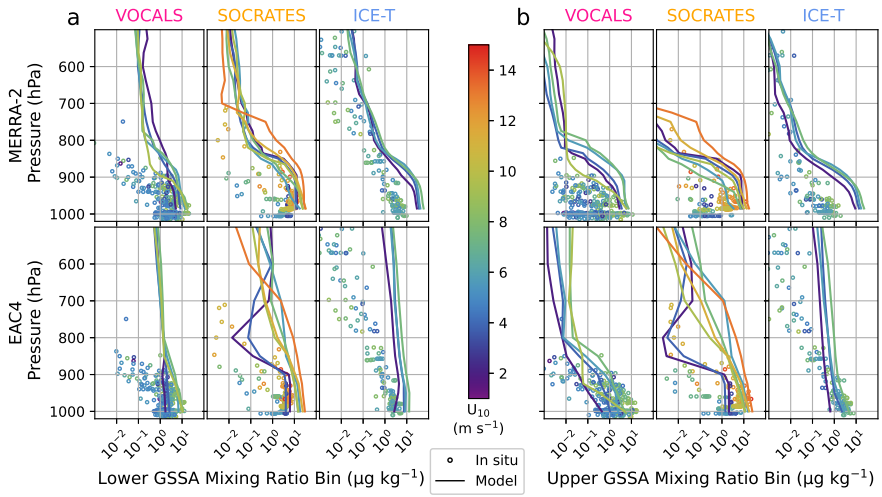


Fig. 3 *In situ* observations of $GSSA_{\mathrm{MR}}$ (hollow circles) are compared to profiles of $GSSA_{\mathrm{MR}}$ for the two largest bins from MERRA-2 and EAC4 for each field campaign (lines). Both are colored by U_{10}. The vertical profiles are taken for each corresponding time and location from the *in situ* observations and then averaged by U_{10} bins of 2 m s^{-1}. Note that the X-axis is on a log-10 scale.

this study only extend to r_{d}=1 µm, and therefore a small portion of particle sizes from the AERMR02 bin (0.25<r_{d}<1 µm) are neglected from the *in situ* when compared to the EAC4 AERMR02 bin.

Using the geographic locations of each sample from VOCALS, SOCRATES, and ICE-T, the corresponding reanalysis $GSSA_{\mathrm{MR}}$s were compared to each *in situ* sample using the closest time-step, latitude, and longitude. All pressure levels within the model were used to generate the mean vertical profiles of $GSSA_{\mathrm{MR}}$ for U_{10} bins of 2 m s^{-1}. Figure 3 compares the average model predicted $GSSA_{\mathrm{MR}}$ vertical profiles to individual *in situ* $GSSA_{\mathrm{MR}}$s for both the respective lower (Fig. 3a) and upper (Fig. 3b) $GSSA_{\mathrm{MR}}$ bins for both reanalysis products; MERRA-2 (top row) and EAC4 (bottom row).

On average, both MERRA-2 and EAC4 overestimate $GSSA_{\mathrm{MR}}$s for both bins across a majority of wind speeds, although EAC4 appears most realistic for the upper $GSSA_{\mathrm{MR}}$ bin (AERM03), and more representative of the boundary layer of all three locations and bins than MERRA-2. It's possible that the lack of observed particles sizes r_{d}> 1 µm may contribute to the discrepancy between the lower bin of EAC4 and *in situ* $GSSA_{\mathrm{MR}}$s, however, it's unlikely the mass from these particles contributes significantly due to the mass given the G-Mean_M is centered above 2 µm.

Both models appear to significantly overestimate the vertical mixing of these particles into the free troposphere. MERRA-2 average vertical profiles appear better at constraining the vertical mixing of both SSA bins for all locations, with a sharp reduction in $GSSA_{\mathrm{MR}}$s with decreasing pressure above the average MBL, however, MERRA-2 appears to be over-representing the depth of the average MBL of all three regions compared to the ERA5 MBL depths (Fig. 2b, 2j). EAC4 appears to mix these particles well above the MBL for all regions for the lower $GSSA_{\mathrm{MR}}$ bin, but does appear to capture more of a drop off of these particles in the upper $GSSA_{\mathrm{MR}}$ bin for

VOCALS and SOCRATES. However, EAC4 still significantly overmixes these particles for the convective ICE-T region for both the lower and upper $GSSA_{\mathrm{MR}}$ bins, showing nearly linear profiles into the free troposphere.

5 Quantitative bias of models vs. *in situ* mixing ratios

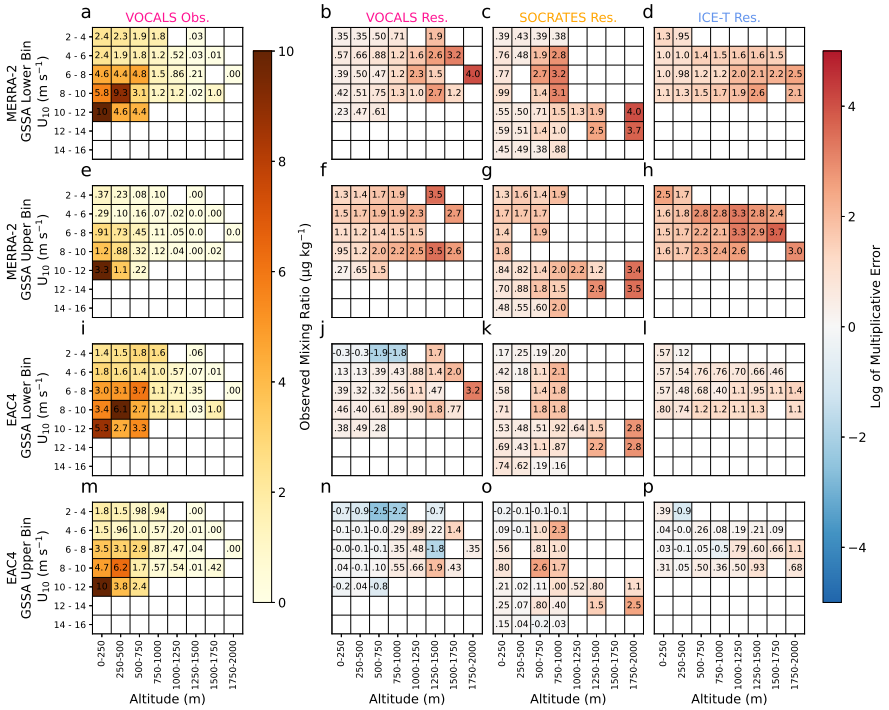


Fig. 4 A quantitative assessment of the model biases for $GSSA_{\mathrm{MR}}$ for both reanalysis products at different altitudes and 2 m s^{-1} U_{10} wind speed bins is shown for all three campaigns. The first column is the observed $GSSA_{\mathrm{MR}}$s for VOCALS to provide a general context for $GSSA_{\mathrm{MR}}$s biases. SOCRATES and ICE-T *in situ* $GSSA_{\mathrm{MR}}$s can be seen in the Extended Data. Each box within the grid represents the logarithmic bias on a base-10 scale for modeled $GSSA_{\mathrm{MR}}$ minus the average observed $GSSA_{\mathrm{MR}}$ for each wind speed bin (y-axis) and altitude (x-axis). Empty boxes indicate no data present for that campaign under those conditions. Red indicates the model is overestimating the $GSSA_{\mathrm{MR}}$, while blue indicates the model is underestimating the $GSSA_{\mathrm{MR}}$. Note that when the $GSSA_{\mathrm{MR}}$ drops below 1 μg kg^{-1}, the zero placeholder to the left of the decimal is removed for sake of space.

Next, we evaluate the model performance using a base-10 logarithmic bias, defined as $\log_{10}$(Modeled/Observed). Figure 4 shows the $GSSA_{\mathrm{MR}}$ biases for 2 m s^{-1} U_{10} wind speed bins and altitudes for all three campaigns and both models' $GSSA_{\mathrm{MR}}$ bins, as well as the observed $GSSA_{\mathrm{MR}}$s for the VOCALS campaign (first column). The observed $GSSA_{\mathrm{MR}}$s for the other two campaigns, as well as VOCALS, can be seen in

the Extended Data (Figure 2). The difference between Figure 4 and Figure 3 is that the lines in Figure 3 are vertical profiles taken for every geographic location that a sample occurred, whereas Figure 4 contains model predicted $GSSA_{\mathrm{MR}}$s for only geographic locations and pressure levels where *in situ* samples were taken. Bins left blank indicate there were no *in situ* samples observed for that altitude and U_{10} combination.

Overall, there exists a range of accuracies between both models, U_{10} bins, and altitudes, but both models appear to have the smallest biases for the lower to middle wind speeds and lowest altitudes. MERRA-2 performance across U_{10} appears to ubiquitously overestimate both $GSSA_{\mathrm{MR}}$ bins for all locations. Most starkly, MERRA-2 appears to overmix both $GSSA_{\mathrm{MR}}$ bins with altitude, with the largest discrepancies found at high altitudes and high U_{10} conditions. Overall, MERRA-2 seems to overestimate VOCALS, SOCRATES, and ICE-T for the smallest $GSSA_{\mathrm{MR}}$ bin by an average of 1.17, 1.43, and 1.53 orders of magnitude respectively, and the largest $GSSA_{\mathrm{MR}}$ bin increases in bias with averages of 1.76, 1.60, and 2.38 orders of magnitude overestimation, respectively.

Unlike MERRA-2, the performance of EAC4 does vary with U_{10}. EAC4 appears to underestimate both $GSSA_{\mathrm{MR}}$s for the weakest U_{10} of VOCALS, and the largest $GSSA_{\mathrm{MR}}$s for SOCRATES. Overall, there appears to be a clear bias in EAC4 for each altitude and wind speed, but not a clear linear relationship with U_{10}. EAC4 seems to suffer similarly to MERRA-2 in the overmixing of $GSSA_{\mathrm{MR}}$s to higher altitudes and at stronger U_{10}. Overall, EAC4 seems to overestimate VOCALS, SOCRATES, and ICE-T for the smallest $GSSA_{\mathrm{MR}}$ bin by an average of 0.56, 1.01, and 0.81, orders of magnitude respectively, while the largest $GSSA_{\mathrm{MR}}$ bin sees an overall decrease in bias from the smallest bin with values of -0.09, 0.65, and 0.26 orders of magnitude, respectively.

6 Uncertainty in the treatment of giant sea salt

Uncertainty in $GSSA_{\mathrm{MR}}$ estimates in these models can stem from three main variables: the sea salt aerosol source functions (SSSFs), the vertical mixing parameters, and then removal mechanisms like wet and dry deposition schemes. A variety of combinations of these parameters may generate seemingly realistic results when assessing model averages or climatic scale distributions, but ultimately have unrealistic results when comparing these modeled $GSSA_{\mathrm{MR}}$ to *in situ* observations over a range of wind speeds and environmental conditions. Examining these parameters individually within the context of GSSA particles will be essential to improving model performance.

There is still wide variety of SSSFs implemented in global models [57]. Model aerosol reanalysis products like EAC4 and MERRA-2 utilize the Monahan 1986 [54] (M86) and Gong 2003 [51] (G03) source functions respectively to represent SSA production. Deeper investigation into these source functions reveal that their derivation and intended applications remain unclearly defined. M86 used satellites and laboratory experiments to derive an interfacial SSA source function, or source function representative of the very near the air-sea interface, from measurements mere centimeters above the wave surface (0.01-0.07 m). Then, G03 adapted this interfacial source function

into an effective source function, or source function that represents the number of particles that enter the mixed layer of the MBL, by tuning it to open ocean observations taken by ship at 18 m above sea level from the North Sea to better represent particles $\leq$0.2 µm [58]. Therefore, the G03 source function was not tuned with larger particles in mind, and the data used for tuning only extends through particles of $r_d \leq 2.7$ µm.

Mixing of these particles is also essential, not only to accurately represent $GSSA_{MR}$s across separate pressure levels, but to also ensure that the total aerosol column mass is realistic. Both models overmix GSSA into the free troposphere when compared to observations, implying there is likely improvement needed in the vertical transport of these particles, which is highly non-trivial. GSSA within the average MBL will likely remain in their deliquesced state, making them predominately spherical particles with a mass and volume dominated by water (between 2-8 times the mass of the dry salt particle [59]). If they are mixed into dryer free-tropospheric air, these particles equilibrate to these lower RHs, losing significant mass and becoming irregularly shaped particles whose atmospheric transport and settling may be more similar to dust particles. Additionally, overmixing too quickly may result in artificially depleted surface $GSSA_{MR}$s, which may explain the negative bias seen in EAC4 at lower altitudes - rapid vertical transport of these particles away from the surface may deplete surface $GSSA_{MR}$s too quickly, ultimately generating $GSSA_{MR}$s aloft that are significantly higher than observations. This, in combination with over-production from SSSFs at the surface, may result in seemingly realistic near-surface $GSSA_{MR}$s but ultimately unrealistically high total SSA column masses.

7 Implications of overestimating giant sea salt aerosol

The results presented here indicate that both MERRA-2 and EAC4 substantially overestimate $GSSA_{MR}$s relative to *in situ* observations, with biases that increase with altitude and wind speed (Fig. 4). Because these reanalysis products are widely used to characterize aerosol distributions and to provide inputs for observational analyses and numerical models, these biases may significantly influence our assessments of GSSA impacts.

Several studies have used MERRA-2 aerosol fields to investigate aerosol–cloud interactions and convective processes[5, 60, 61]. For example, Pan et al. (2022) [60] examined how fine and coarse SSA influence lightning activity in tropical deep convective clouds, finding that increased coarse sea spray promotes the formation of larger droplets, enhances warm rain processes, and suppresses lightning activity. Because GSSA strongly influences cloud droplet formation and precipitation efficiency, an overestimation of GSSA concentrations could potentially amplify the inferred role of these particles in weakening convection or reducing lightning frequency.

A similar consideration applies to studies examining the role of coarse sea spray aerosols in marine warm clouds. Liu et al. (2022) [5] combined satellite observations with SSA concentrations from MERRA-2 to examine how GSSA affects droplet effective radius and precipitation occurrence in marine clouds, concluding that increased GSSA concentrations promote larger droplet sizes and enhance warm-rain formation.

If MERRA-2 overestimates the abundance and vertical mixing of GSSA particles, the relationship between coarse aerosol loading and precipitation may be strengthened by biases in the model dataset itself. Consequently, the sensitivity of marine warm-rain processes to coarse aerosol loading may differ from that suggested by studies relying solely on reanalysis aerosol concentrations.

Reanalysis aerosol products are also increasingly used to initialize or constrain aerosol-aware microphysics schemes in numerical weather prediction models. For example, Yuan et al. (2026) [61] incorporated aerosol fields derived from CAMS into simulations of supercooled liquid water and aircraft icing environments, demonstrating that aerosol loading strongly influences cloud droplet number concentrations, droplet sizes, and cloud lifetime. If GSSA concentrations are overestimated in these datasets, simulations driven by such aerosol fields may produce enhanced warm-rain formation or altered droplet size distributions compared to those that would occur under observed marine aerosol conditions.

These examples highlight the importance of evaluating GSSA representations in reanalysis products when they are used to interpret marine cloud processes or aerosol–precipitation interactions, but implications extend to aerosol direct and indirect forcings in general. Because GSSA particles are hypothesized to play an important role in aerosol-cloud-interactions despite existing in disproportionately small concentrations, even moderate biases in their abundance may affect modeled cloud responses. Incorporating observational constraints on GSSA concentrations may therefore improve the interpretation of aerosol–cloud interactions and help ensure that the role of coarse marine aerosols in atmospheric processes is accurately represented.

Extended Data. Figure 5 is Extended Data demonstrating that across different U_{10} bins there exists very minimal changes in GSSA-SD shape with altitude. This is a complimentary Figure 2 to demonstrate that the vertical distribution of different particle sizes is nearly independent of U_{10} within the mixed layer of the MBL.

Figures 6 shows the average observed $GSSA_{\mathrm{MR}}$ for each field campaign to show original values observed in these campaigns. It should be noted that there were more samples observed in the free troposphere for each field campaigns than were utilized in this study. These samples yielded such low salt loading that it was undetectable by the analysis methods, meaning that the mean $GSSA_{\mathrm{MR}}$s for the free troposphere are likely artificially higher since the null-values have been removed from the averaging. Figure 7 shows the modeled $GSSA_{\mathrm{MR}}$ using the same number of data points per bin as Figure 6.

Acknowledgements. The authors would like to acknowledge the National Science Foundation for funding of this research under award #2145502. The authors would also like to thank the many scientists across the VOCALS, ICE-T, and SOCRATES field campaigns who put in long hours and made the collection of this data possible. Additionally, the authors would like to acknowledge David H. Richter for his insightful conversations at conferences with the lead author Katherine L. Ackerman, that ultimately lead to research question explored in this paper.

Author Contributions. K.A. designed the experiments, wrote the code and prepared the figures, and wrote the initial manuscript. J.J. collected the in situ data. J.J.

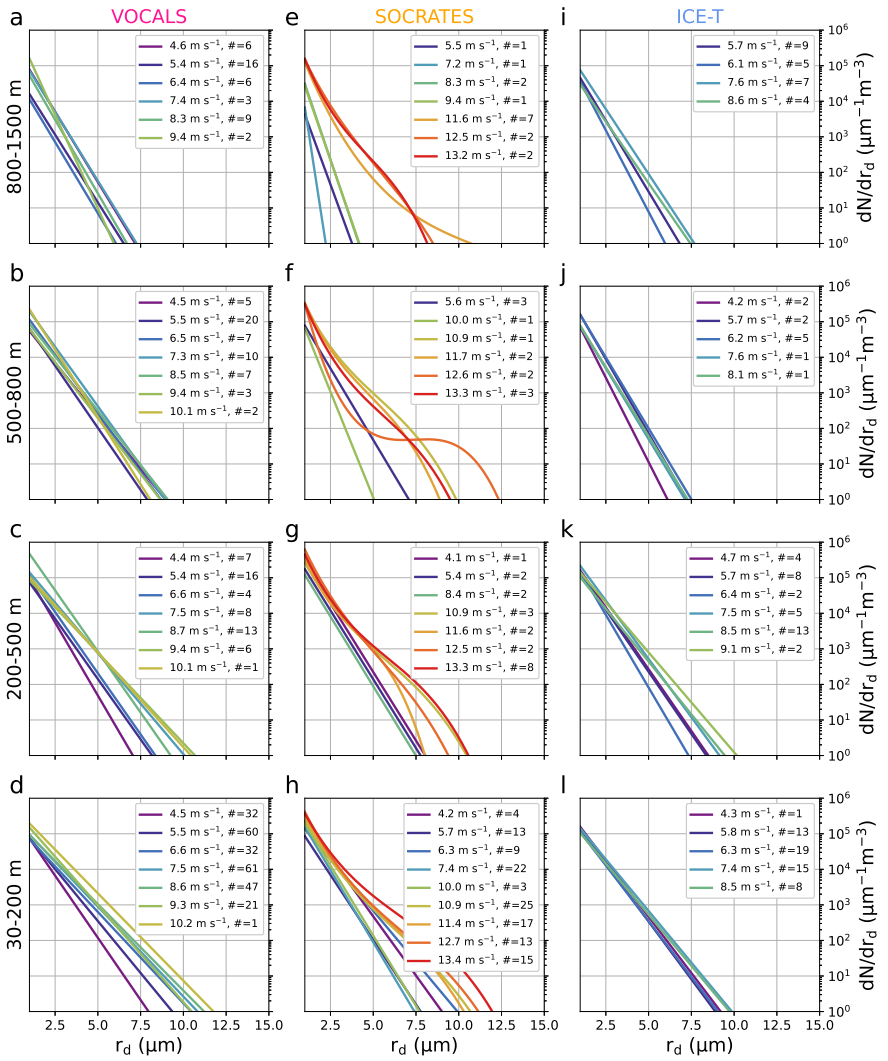


Fig. 5 GSSA-SDs for SOCRATES, VOCALS, and ICE-T are shown for four altitude bins (30-200 m, 200-500 m, 500-800 m, and 800-1500 m), with average size distributions per 1 m s^{-1} U_{10} bins (colors). For GSSA-SDs observed in $<$ 10 m s^{-1} U_{10} conditions, these are fit using an exponential decay, while GSSA-SDs observed in $>$ 10 m s^{-1} U_{10} conditions are fit using a 3rd-order polynomial. The U_{10} bins are labeled on each graph along with how many samples make up the average GSSA-SD for that graph.

and A.N. helped guide questions for the experiments, and edited the manuscript. All authors reviewed the manuscript.

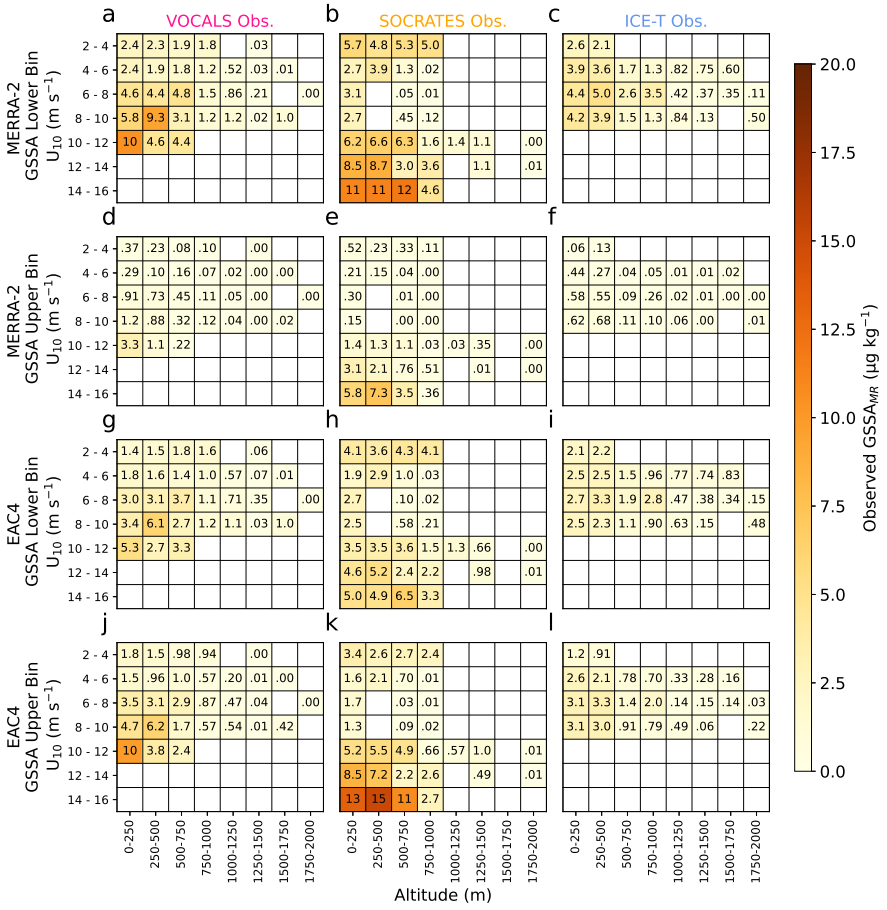


Fig. 6 Average observed $GSSA_{\mathrm{MR}}$s across each field campaign for various altitude and U_{10} bins for the different $GSSA_{\mathrm{MR}}$ bins of both models. Blank bins indicate there are no observations for that wind speed and altitude bin. The first column in this figure is identical to Figure 4 in the paper. The colorbar has been adapted to represent only positive values.

References

[1] Xu, W. *et al.* Sea spray as an obscured source for marine cloud nuclei. *Nature Geoscience* **15**, 282–286 (2022). URL https://www.nature.com/articles/s41561-022-00917-2.

[2] Fairall, C. W. The effect of sea spray on surface energy transports over the ocean (1994). URL https://cir.nii.ac.jp/crid/1370285708267872403.bib?lang=en.

[3] Andreas, E. L. Sea spray and the turbulent air-sea heat fluxes. *Journal of Geophysical Research* **97** (1992).

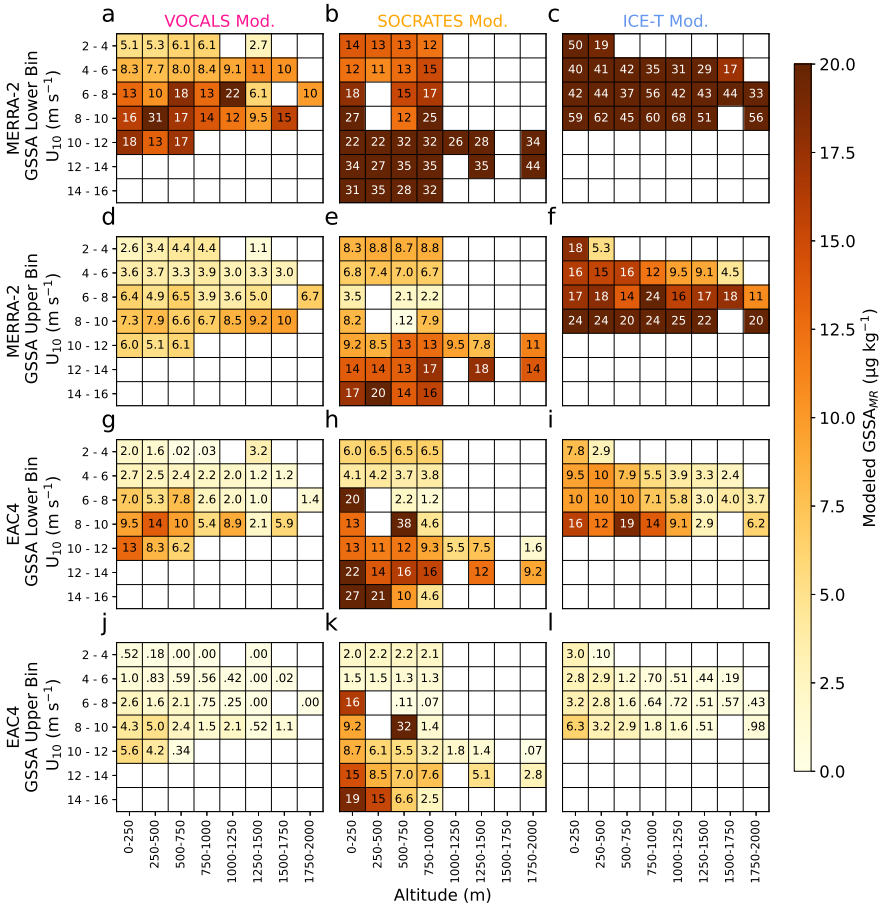


Fig. 7 Average modeled $GSSA_{\mathrm{MR}}$s across each field campaign for various altitude and U_{10} bins for the different $GSSA_{\mathrm{MR}}$ bins of both models. These averaged modeled $GSSA_{\mathrm{MR}}$s are only for points in time and space where observations from each field campaign occurred. Blank bins indicate there are no observations for that wind speed and altitude bin.

[4] Jensen, J. B. & Lee, S. Giant sea-salt aerosols and warm rain formation in marine stratocumulus. *Journal of the Atmospheric Sciences* **65**, 3678–3694 (2008).

[5] Liu, F. *et al.* Opposing comparable large effects of fine aerosols and coarse sea spray on marine warm clouds. *Communications Earth and Environment* **3** (2022).

[6] Andreas, E. L. The Temperature of Evaporating Sea Spray Droplets. *Journal of Atmospheric Sciences* **52**, 852–862 (1995). URL https://journals.ametsoc.org/view/journals/atsc/52/7/1520-0469_1995_052_0852_ttoess_2_0_co_2.xml.

[7] Pravia-Sarabia, E., Gomez-Navarro, J. J., Jimenez-Guerrero, P. & Montavez, J. P. Influence of sea salt aerosols on the development of Mediterranean tropical-like

cyclones. *Atmospheric Chemistry and Physics* **21**, 13353–13368 (2021).

[8] Lewis, E. R. & Schwartz, S. E. *Sea Salt Aerosol Production: Mechanisms, Methods, Measurements, and Models* Vol. 152 (American Geophysical Union, 2004).

[9] Watson-Parris, D. & Smith, C. J. Large uncertainty in future warming due to aerosol forcing. *Nature Climate Change* **12**, 1111–1113 (2022).

[10] Cooper, W. A., Lasher-Trapp, S. G. & Blyth, A. M. The influence of entrainment and mixing on the initial formation of rain in a warm cumulus cloud. *Journal of the Atmospheric Sciences* **70**, 1727–1743 (2013).

[11] Jensen, J. B. & Nugent, A. D. Condensational growth of drops formed on giant sea-salt aerosol particles. *Journal of the atmospheric sciences* **74**, 679–697 (2017).

[12] Lasher-trapp, S. G., Cooper, W. A. & Blyth, A. M. Broadening of droplet size distributions from entrainment and mixing in a cumulus cloud. *Quarterly Journal of the Royal Meteorological Society* **131**, 195–220 (2005).

[13] Twomey, S. Pollution and the planetary albedo. *Atmospheric Environment (1967)* **8**, 1251–1256 (1974).

[14] Albrecht, B. A. Aerosols, cloud microphysics, and fractional cloudiness. *Science* **245**, 1227–1230 (1989).

[15] Ackerman, A. S. *et al.* Reduction of tropical cloudiness by soot. *Science* **288**, 1042–1047 (2000).

[16] Posselt, R. & Lohmann, U. Influence of Giant CCN on warm rain processes in the ECHAM5 GCM. *Atmospheric Chemistry and Physics* **8**, 3769–3788 (2008).

[17] L'Ecuyer, T. S., Berg, W., Haynes, J., Lebsock, M. & Takemura, T. Global observations of aerosol impacts on precipitation occurrence in warm maritime clouds. *Journal of Geophysical Research Atmospheres* **114**, 1–15 (2009).

[18] Jung, E. *et al.* Precipitation effects of giant cloud condensation nuclei artificially introduced into stratocumulus clouds. *Atmospheric Chemistry and Physics* **15**, 5645–5658 (2015).

[19] Dror, T. *et al.* Sensitivity of warm clouds to large particles in measured marine aerosol size distributions-a theoretical study. *Atmospheric Chemistry and Physics* **20**, 15297–15306 (2020).

[20] Dziekan, P., Jensen, J. B., Grabowski, W. W. & Pawlowska, H. Impact of Giant Sea Salt Aerosol Particles on Precipitation in Marine Cumuli and Stratocumuli: Lagrangian Cloud Model Simulations. *Journal of the Atmospheric Sciences* **78**, 4127–4142 (2021).

[21] Fossum, K. N. *et al.* Sea-spray regulates sulfate cloud droplet activation over oceans. *npj Climate and Atmospheric Science* **3** (2020). URL http://dx.doi.org/10.1038/s41612-020-0116-2.

[22] Hoffmann, F. & Feingold, G. Cloud microphysical implications for marine cloud brightening: The importance of the seeded particle size distribution. *Journal of the Atmospheric Sciences* 3247–3262 (2021).

[23] Rosenfeld, D., Lahav, R., Khain, A. & Pinsky, M. The role of sea spray in cleansing air pollution over ocean via cloud processes. *Science* **297**, 1667–1670 (2002).

[24] Blanchard, D. C., Woodcock, A. H. & Cipriano, R. J. The vertical distribution of the concentration of sea salt in the marine atmosphere near Hawaii (Oahu). *Tellus, Series B* **36 B**, 118–125 (1984).

[25] Reid, J. S., Jonsson, H. H., Smith, M. H. & Smirnov, A. Evolution of the vertical profile and flux of large sea-salt particles in a coastal zone. *Journal of Geophysical Research Atmospheres* **106**, 12039–12053 (2001).

[26] Lenain, L. & Melville, W. K. Evidence of Sea-State Dependence of Aerosol Concentration in the Marine Atmospheric Boundary Layer. *Journal of Physical Oceanography* **47**, 69–84 (2017). URL https://journals.ametsoc.org/view/journals/phoc/47/1/jpo-d-16-0058.1.xml.

[27] Schlosser, J. S. *et al.* Relationships Between Supermicrometer Sea Salt Aerosol and Marine Boundary Layer Conditions: Insights From Repeated Identical Flight Patterns. *Journal of Geophysical Research: Atmospheres* **125**, 1–17 (2020).

[28] Gonzalez, M. E. *et al.* Relationships between supermicrometer particle concentrations and cloud water sea salt and dust concentrations: analysis of MONARC and ACTIVATE data. *Environmental Science: Atmospheres* **2**, 738–752 (2022).

[29] Woodcock, A. H. & Gifford, M. M. Sampling atmospheric sea-salt nuclei over the ocean. *Journal of Marine Research* **8** (1949).

[30] McNaughton, C. S. *et al.* Results from the dc-8 inlet characterization experiment (dice): Airborne versus surface sampling of mineral dust and sea salt aerosols. *Aerosol Science and Technology* **41**, 136–159 (2007).

[31] Noone, K. J., Ogren, J. A., Heintzenberg, J., Charlson, R. J. & Covert, D. S. Design and calibration of a counterflow virtual impactor for sampling of atmospheric fog and cloud droplets. *Aerosol Science and Technology* **8**, 235–244 (1988).

[32] Huebert, B. J. *et al.* Pelti: Measuring the passing efficiency of an airborne low turbulence aerosol inlet. *Aerosol Science and Technology* **38**, 803–826 (2004).

[33] Wilson, J. C. *et al.* Function and performance of a low turbulence inlet for sampling supermicron particles from aircraft platforms. *Aerosol Science and Technology* **38**, 790–802 (2004).

[34] Quinn, P. K. *et al.* Surface submicron aerosol chemical composition: What fraction is not sulfate? *Journal of Geophysical Research Atmospheres* **105**, 6785–6805 (2000).

[35] Russell, L. M. & Singh, E. G. Submicron salt particle production in bubble bursting. *Aerosol Science and Technology* **40**, 664–671 (2006).

[36] Woodcock, A. H. Salt Nuclei in Marine Air As a Function of Altitude and Wind Force (1953).

[37] Modini, R. L. *et al.* Primary marine aerosol-cloud interactions off the coast of California. *Journal of Geophysical Research: Atmospheres* **120**, 4282–4303 (2015). URL https://agupubs.onlinelibrary.wiley.com/doi/10.1002/2014JD022963.

[38] Quinn, P., Coffman, D., Johnson, J., Upchurch, L. & Bates, T. Small fraction of marine cloud condensation nuclei made up of sea spray aerosol. *Nature Geoscience* **10**, 674–679 (2017).

[39] Saliba, G. *et al.* Factors driving the seasonal and hourly variability of sea-spray aerosol number in the North Atlantic. *Proceedings of the National Academy of Sciences* **116**, 20309–20314 (2019). URL https://pnas.org/doi/full/10.1073/pnas.1907574116.

[40] Dedrick, J. L., Saliba, G., Williams, A. S., Russell, L. M. & Lubin, D. Retrieval of the Sea Spray Aerosol Mode from Submicron Particle Size Distributions and Supermicron Scattering during LASIC (2022). URL https://amt.copernicus.org/preprints/amt-2022-46/amt-2022-46.pdf.

[41] Clarke, A. *et al.* Sea-salt size distribution from breaking waves: Implications for marine aerosol production and optical extinction measurements during SEAS. *Journal of Atmospheric and Oceanic Technology* **20**, 1362–1374 (2003).

[42] Clarke, A. D., Owens, S. R. & Zhou, J. An ultrafine sea-salt flux from breaking waves: Implications for cloud condensation nuclei in the remote marine atmosphere. *Journal of Geophysical Research Atmospheres* **111**, 1–14 (2006).

[43] Xu, W. *et al.* Seasonal Trends of Aerosol Hygroscopicity and Mixing State in Clean Marine and Polluted Continental Air Masses Over the Northeast Atlantic. *Journal of Geophysical Research: Atmospheres* **126** (2021). URL https://agupubs.onlinelibrary.wiley.com/doi/10.1029/2020JD033851.

[44] Russell, L. M., Moore, R. H., Burrows, S. M. & Quinn, P. K. Ocean flux of salt, sulfate, and organic components to atmospheric aerosol. *Earth-Science Reviews*

239, 104364 (2023). URL https://doi.org/10.1016/j.earscirev.2023.104364.

[45] Wood, R. *et al.* The vamos ocean-cloud-atmosphere-land study regional experiment (vocals-rex): goals, platforms, and field operations. *Atmospheric Chemistry and Physics* **11**, 627–654 (2011).

[46] McFarquhar, G. M. *et al.* Observations of clouds, aerosols, precipitation, and surface radiation over the southern ocean: An overview of capricorn, marcus, micre, and socrates. *Bulletin of the American Meteorological Society* **102**, E894–E928 (2021).

[47] Jensen, J. B. *et al.* The giant nucleus impactor (gni)—a system for the impaction and automated optical sizing of giant aerosol particles with emphasis on sea salt. part i: Basic instrument and algorithms. *Journal of Atmospheric and Oceanic Technology* **37**, 1551–1569 (2020).

[48] Ranz, W. E. & Wong, J. Impaction of dust and smoke particles on surface and body collectors. *Industrial & Engineering Chemistry* **44**, 1371–1381 (1952).

[49] Taing, C., Ackerman, K. L., Nugent, A. D. & Jensen, J. B. A New Instrument for Determining the Coarse-Mode Sea Salt Aerosol Size Distribution. *Journal of Atmospheric and Oceanic Technology* 1935–1947 (2021).

[50] Tang, I. N., Tridico, A. & Fung, K. Thermodynamic and optical properties of sea salt aerosols. *Journal of Geophysical Research: Atmospheres* **102**, 23269–23275 (1997).

[51] Gong, S. A parameterization of sea-salt aerosol source function for sub-and super-micron particles. *Global biogeochemical cycles* **17** (2003).

[52] Randles, C. A. *et al.* The merra-2 aerosol reanalysis, 1980 onward. part i: System description and data assimilation evaluation. *Journal of Climate* **30**, 6823–6850 (2017).

[53] Inness, A. *et al.* The cams reanalysis of atmospheric composition. *Atmospheric Chemistry and Physics* **19**, 3515–3556 (2019).

[54] Monahan, E. C., Spiel, D. E. & Davidson, K. L. *A Model of Marine Aerosol Generation Via Whitecaps and Wave Disruption*, 167–174 (Springer Netherlands, Dordrecht, 1986). URL https://doi.org/10.1007/978-94-009-4668-2_16.

[55] Yang, X. Cams global sea salt aerosol mixing ratios. https://confluence.ecmwf.int/display/CKB/CAMS+global+sea+salt+aerosol+mixing+ratios (2023). Last modified by Michela Giusti; accessed 2026-01-30.

[56] Hersbach, H. *et al.* The ERA5 global reanalysis. *Quarterly Journal of the Royal Meteorological Society* **146**, 1999–2049 (2020). URL https://rmets.onlinelibrary.

wiley.com/doi/10.1002/qj.3803.

[57] Song, A., Li, J., Tsona, N. T. & Du, L. Parameterizations for sea spray aerosol production flux. *Applied Geochemistry* 105776 (2023).

[58] O'Dowd, C. D., Smith, M. H., Consterdine, I. E. & Lowe, J. A. Marine aerosol, sea-salt, and the marine sulphur cycle: A short review. *Atmospheric Environment* **31**, 73–80 (1997).

[59] Reich, O., Gleichweit, M. J., David, G., Leemann, N. & Signorell, R. Hygroscopic growth of single atmospheric sea salt aerosol particles from mass measurement in an optical trap. *Environmental Science: Atmospheres* **3**, 695–707 (2023).

[60] Pan, Z. *et al.* Coarse sea spray inhibits lightning. *Nature Communications* **13** (2022).

[61] Yuan, M. *et al.* Quantitative assessment of supercooled liquid water sensitivity to different aerosol field inputs over the sichuan basin. *Atmospheric Chemistry and Physics* **26**, 2275–2292 (2026).